Electronic Supplementary Material (ESI) for Reaction Chemistry & Engineering.

Rapid Optimisation of API Crystallisation in a Segmented Flow Reactor with a Continuous, Variable Temperature Gradient

Supplementary Information

Karen Robertson,*[a], [b] Peter H. Seeberger[b] [c] and Kerry Gilmore*[b], [d]

[a] Dr. Karen Robertson
Faculty of Engineering
University of Nottingham NG7 2RD (UK)
Email: Karen.Robertson@nottingham.ac.uk

[b] Dr. Karen Robertson, Prof. Dr. P. H. Seeberger, Prof. Dr. K. Gilmore
Department of Biomolecular Systems
Max Planck Institute of Colloids and Interfaces
Am Mühlenberg 1, 14476 Potsdam (Germany)
E-mail: peter.seeberger@mpikg.mpg.de

[c] Prof. Dr. P. H. Seeberger
Department of Chemistry and Biochemistry
Freie Universität Berlin
Arnimallee 22, 14195 Berlin (Germany)

[d] Prof. Dr. K. Gilmore
University of Connecticut
Storrs, CT 06269 (United States)
E-mail: kerry.m.gilmore@uconn.edu

Contents

1. Description of KRAIC-G 3
2. Temperature measurements 4
3. Paracetamol crystallisaion 7

1. Description of KRAIC-G

Figures S1 and S2a show an image of the full set-up and a close-up IR image, respectively.

The KRAIC-G comprises five independently temperature-controlled zones, depicted in Figure S2b. The feed stock is heated *via* a standard hotplate stirrer and oil bath. Transfer tubing between the feed stock, pump, mixer and reactor are heated through an air-filled jacketed tubing, the outer tubing of which is heated electrically. The pump and mixer sections are independently temperature controlled through custom heating blocks of aluminium and cartridge heating units (Figure S2c). The tubing coil portion of the gradient reactor is an aluminium outer sleeve with a spiral wound groove to insert the FEP tubing coil and an inner polypropylene (PP) core with complementary spiral wound groove through which the cooling fluid flows in an opposing direction to the flow. The base of the aluminium block is heated through six cartridge heaters whilst the cooling fluid enters the top, cooling the reactor in opposition to the cartridge heaters. The flow rate of the cooling fluid is maintained through a by-pass system the by-pass fluid returns directly to the circulator bath, reducing the power required to maintain the outlet temperature after heating of the cooling fluid within the gradient crystalliser.

The solution is delivered through a HNPM-mzr-2521X1 microfluidic gear pump from Darwin microfluidics. Gas delivery is achieved *via* a Bronkhorst EL-Flow mass flow controller. Carrier fluid is delivered by a Harvard Apparatus syringe pump. These media delivery apparatus provide a highly stable flow with very regular slug sizes as can be seen in Figure S2d.

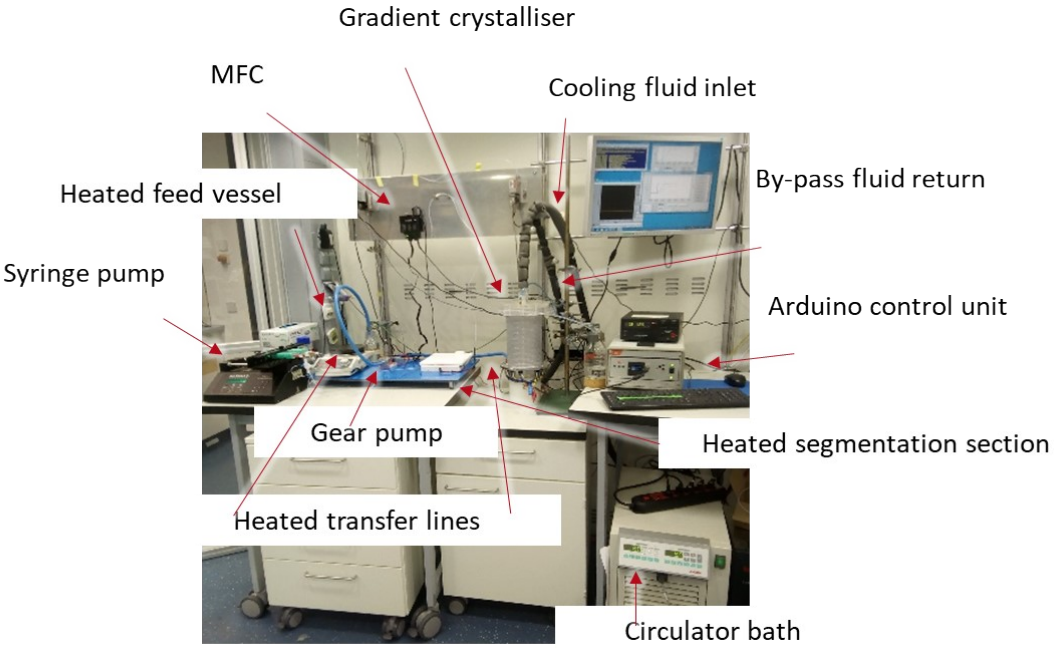

Figure S1 Full image of gradient crystalliser set-up. N.B. MFC – mass flow controller for N_2 delivery

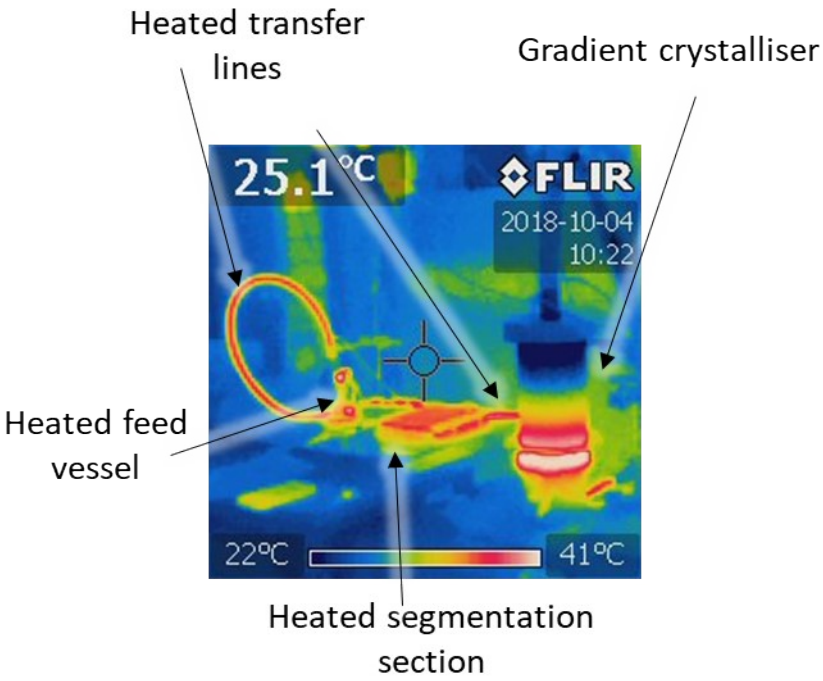

a.

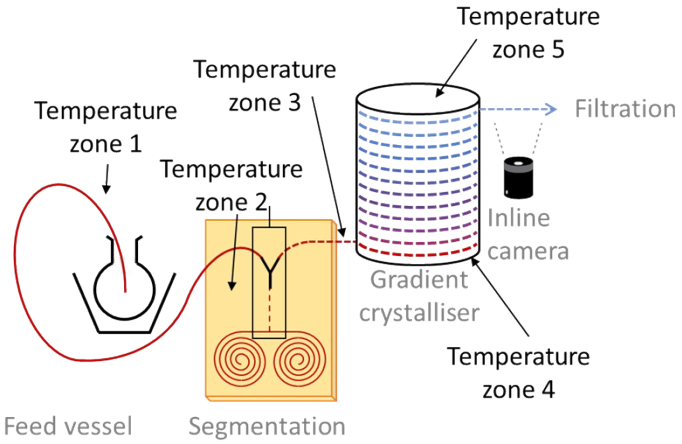

b.

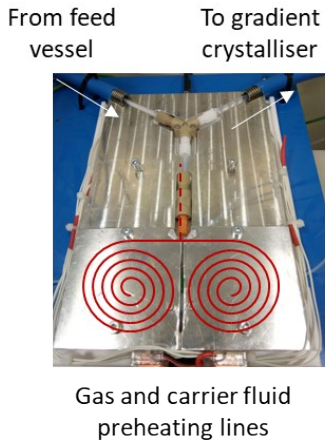

c.

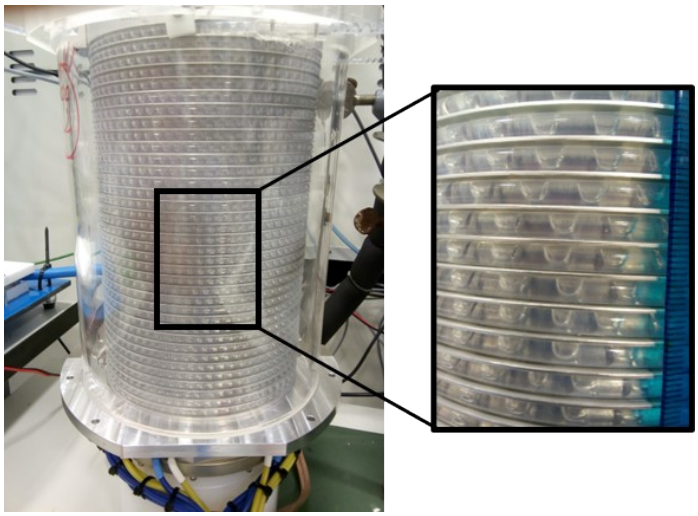

d.

Figure S2 Images of the KRAIC-G. a. IR camera image of the KRAIC-G showing temperature control, b. schematic showing the independently controlled temperature regions, c. segmentation section section with top plate exposed to show fluidic lines, d. gradient crystalliser with segmented flow

2. Temperature measurements

The temperature within the KRAIC-G was measured non-invasively using a FLIR E4 IR thermal imaging camera. The centre spot was focussed on the tubing to ensure the most representative reading (Figure S3).

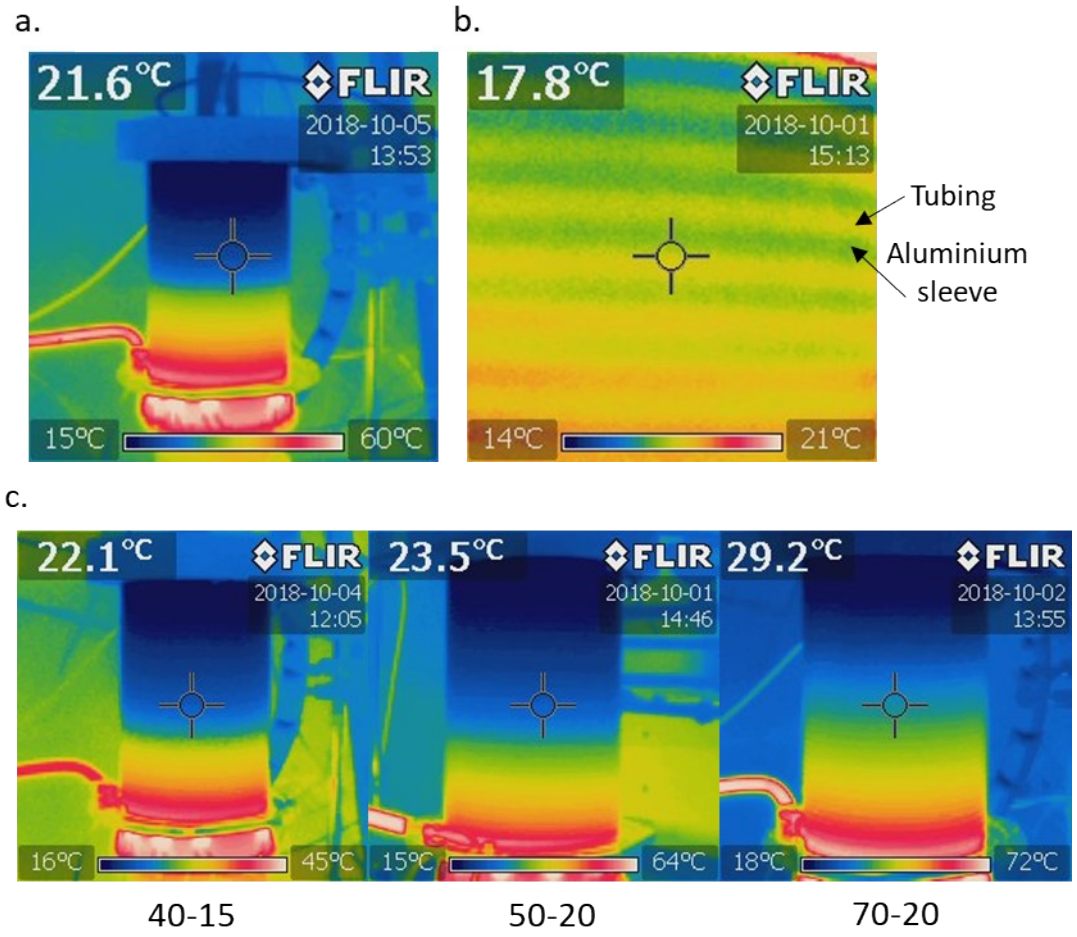

Figure S3a. FLIR image of the gradient crystalliser with a temperature gradient of 55-15 °C, b. close-up image showing the temperature discrepancy between tubing and aluminium sleeve, c. comparison of thermal gradients seen in IR images for varied start and end temperatures

Calibration of the thermal gradients for steady-state (SS) operation was typically carried out with a pure water flow (Table S1, Figure S4) whilst tri-segmented flow as described in the MS was used for calibration of the non-steady state thermal gradient (see MS, Table S2).

Table S1 Calibration parameters for steady-state gradient in the KRAIC-G, N.B. all aqueous runs were performed at a net rate of 2.1 ml/min except *40-15 which was 7 ml/min. All tr-segmented runs were 3.5 ml/min

Start temperature (°C)	End temperature (°C)	Media
60	40	Tri-segmented
80	20	Tri-segmented

70	20	Aqueous
60	20	Aqueous
55	20	Aqueous
50	20	Aqueous
40	20	Aqueous
40	20	Tri-segmented
80	15	Tri-segmented
65	15	Aqueous
55	15	Aqueous
45	15	Aqueous
45	15	Aqueous
40	15	Aqueous

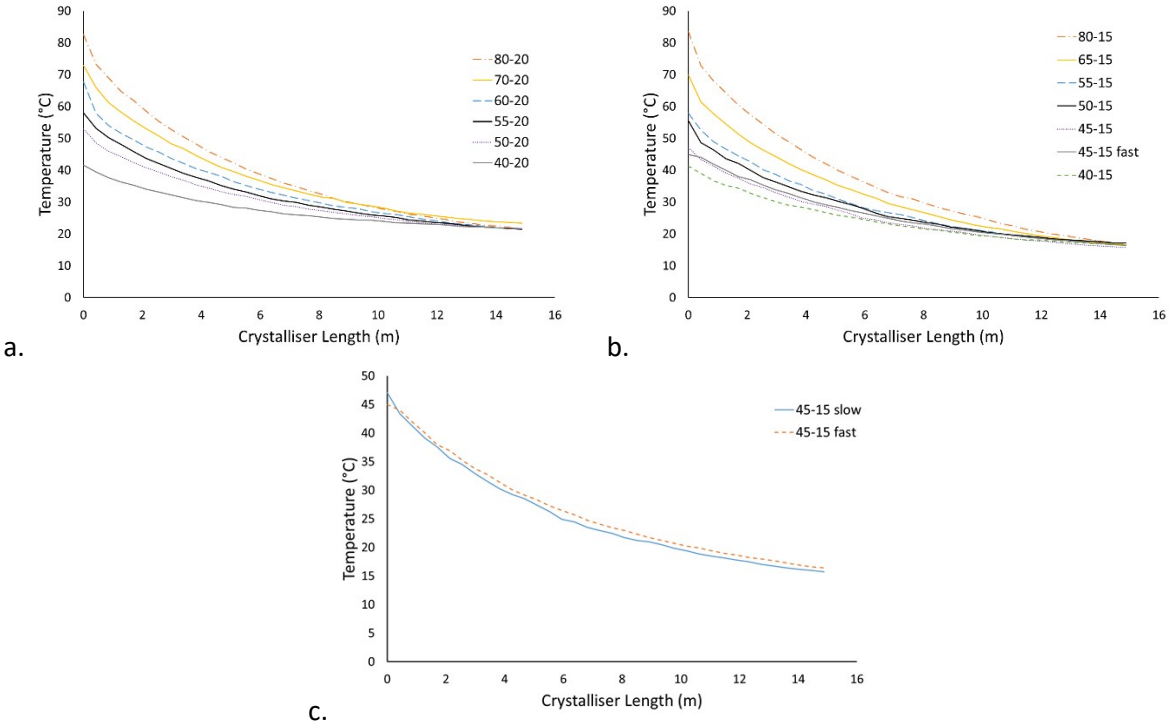

Figure S4 Temperature ramps for steady-state operation of the KRAIC-G. a. Varied start temperature, all with a final temperature of 20 °C, b. varied start temperature, all with a final temperature of 15 °C, c. comparison of net flow 2.1 ml/min (slow) and 7 ml/min (fast)

Table S2. Average hot and cold end temperature ramps measured until setpoint achieved

Set ramp rate (°C/min)	**Average ramp rate measured until setpoint achieved (°C/min)**	
	Hot	**Cold**
0.5	0.52	0.24
1.0	0.94	0.28
5.0	2.2	0.32
10	2.6	0.32

Table S3. Average temperature ramp achieved across the KRAIC-G. N.B. the minimum temperature of ramps 5 and 10 °C/min was achieved for 0.85 m within the first 10 min of experiment, the true maximum ΔT/min values were 2.2 and 2.8 °C/min respectively. Standard deviation are shown in brackets

Crystalliser length (m)	Temperature ramp (°C/min)			
	0.5	1	5	10
0.85	0.45 (0.21)	0.80 (0.28)	0.88 (0.96)	1.09 (1
2.13	0.35 (0.17)	0.67 (0.22)	0.78 (0.76)	0.86 (0
3.40	0.28 (0.18)	0.53 (0.24)	0.66 (0.56)	0.72 (0
4.68	0.22 (0.20)	0.45 (0.17)	0.56 (0.46)	0.60 (0
5.95	0.26 (0.15)	0.39 (0.16)	0.46 (0.38)	0.49 (0
7.23	0.24 (0.15)	0.33 (0.14)	0.41 (0.29)	0.40 (0
8.50	0.25 (0.15)	0.29 (0.30)	0.36 (0.27)	0.37 (0
9.78	0.19 (0.11)	0.29 (0.24)	0.32 (0.23)	0.30 (0
11.05	0.18 (0.11)	0.25 (0.21)	0.28 (0.19)	0.27 (0
12.33	0.15 (0.15)	0.24 (0.19)	0.22 (0.23)	0.25 (0
13.60	0.14 (0.16)	0.22 (0.22)	0.20 (0.26)	0.21 (0
14.88	0.14 (0.20)	0.18 (0.20)	0.18 (0.26)	0.20 (0

3. Paracetamol crystallisation

An exploded view of the initial slopes of the temperature gradient presented in Figure 4 is presented in Figure S5a, highlighting the very similar path taken by all crystallisation experiments excluding that of the 40-16 temperature ramp. The supersaturation ratio for a 255 g/L solution under a temperature profile such as that undertaken by the slugs collected at ET 61 is shown in Figure S4b. Solubility data have been taken from, Agnew, L. R. *et al.*, *Crystal Growth & Design* **2017**, *17* (5), 2418-2427.

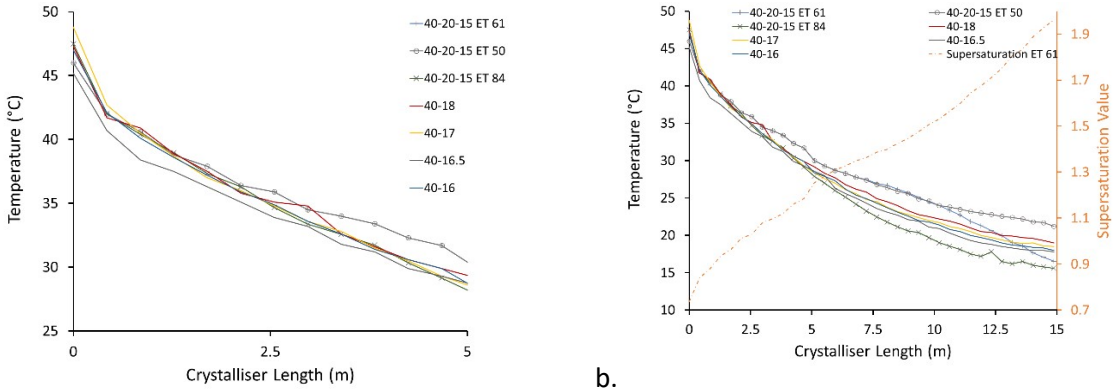

a. b.

Figure S5a exploded view of initial slope in Figure 4b; b. Overlay of supersaturation value for ET 61 temperature profile

Both inline camera and filter paper collection methods were used to identify the extent of crystallisation. As can be seen in Figure S6 and Table S3, there is some discrepancy between the results from the camera and filter paper methods. The depth of field of the lens on the camera may not pick up every crystal, this is a particular challenge for smaller crystals. Conversely, the eluting slugs may spread to separated sections on the filter paper thus providing a source of error at higher levels of crystallisation. The filter paper results are therefore more accurate at lower crystallisation whilst the camera method is more accurate at higher crystallisation.

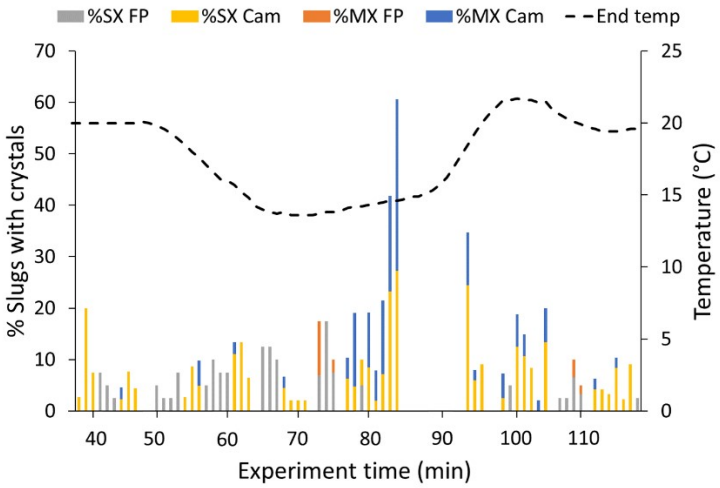

Figure S6 Full data set of crystals identified during NSS paracetamol crystallisation *via* filter paper collection (FP) or inline camera (Cam). Highlighting the percentage of slugs containing single crystals (SX) or multiple crystals (MX). N.B. no data were collected between experiment time 85-93 min

Table S4 Breakdown of crystallisation analysis over a collection period of 4 mins as identified by filter paper collection (FP) or inline camera detection (Cam)

Collection period	**NSS**				**SS 40-17**				**SS 40-18**			
	% slugs		% SX		% slugs		% SX		% slugs		% SX	
	FP	Cam	FP	Cam	FP	Cam	FP	Cam	FP	Cam	FP	Cam
1	9.3	10.3	100	87.6	5.6	3.5	62.5	87.5	3.1	2.1	100	100
2					11.9	8.8	95.0	65.0	5.6	3.9	88.9	81.8
3					15.0	25.9	55.3	53.1	5.6	6.1	88.9	78.6
4					18.8	23.4	81.0	66.7	5.0	2.1	87.5	80.0

Table S5 Crystal size and percentage of rhombohedral plate crystals. Standard deviation shown in brackets for sizing. N.B. rhobohedral is here defined as four sided with ratio of between 0.8-1.3 between side lengths

	Average size of rhombohedral crystal (µm)	**% crys rhombohe**
NSS (57-67 min ET)	541 (0.21)	90
SS 40-17	648 (0.29)	74

SS 40-18	665 (0.21)	70